Efficient Frequency Response Identification for Small Fixed-Wing UAS Using Closed-Loop Flight Data

Justin J. Matt* and Haiyang Chao†
University of Kansas, Lawrence, KS 66045

In this paper, a method to identify bare-airframe, closed-loop, and broken-loop frequency responses from a single set of closed-loop flight data is presented. This approach is particularly useful for small unmanned aircraft, which face unique challenges during system identification flight tests, such as flight safety, open-loop stability, considerable pilot workload during frequency sweep maneuvers, and non-trivial disturbances from atmospheric turbulence. Closed-loop flight testing can address many of these challenges as it improves the stability, repeatability, and flexibility of flight testing, which can lead to higher data quality. The proposed method is demonstrated using simulated data of a small, flying-wing UAS operating in closed-loop in strong turbulence. Frequency responses are identified using a joint input-output method, which prevents bias errors caused by noise feedback. The bare-airframe, closed-loop, and broken-loop frequency responses are identified from one data set with excellent agreement with the simulation truth over a wide frequency range. The example demonstrates the effectiveness of this approach to improve results and reduce flight testing time for small UAS system identification.

I. Introduction

Bare-airframe frequency responses are often identified as an initial step in the aircraft system identification process. Typically, frequency responses are measured from data recorded during open-loop flight maneuvers designed for system identification. Open-loop flight testing is preferred because automatic flight control systems may suppress oscillatory and transient motion that must be excited to yield accurate system identification results. Control systems can also generate control input signals that are highly correlated with each other and/or with external disturbances and noise, which makes it difficult to accurately identify dynamic models. Despite these challenges, there are numerous benefits to studying closed-loop system identification. For example, closed-loop testing may be required for safety reasons, for unstable aircraft, or for aircraft with inherent feedback that cannot be disabled. Additionally, small unmanned aircraft systems (UAS) face unique challenges in system identification that can potentially be addressed through closed-loop testing.

Compared with larger aircraft, it is difficult to perform high-accuracy system identification for small UAS, partially due to their low speeds and light weight. Small UAS are more sensitive to atmospheric disturbances than larger aircraft, which may result in noisy measurement data and necessitate larger, less stable flight maneuvers for accurate identification results [1, 2]. Such maneuvers can be difficult for a pilot to perform from the ground, and automated open-loop maneuvers could result in instability or even loss of control. Atmospheric disturbances also create difficulties repeating maneuvers at the same flight condition (e.g., headwinds and tailwinds can create a vast difference in cruise airspeed). Furthermore, many UAS always operate with some level of automatic control, and so open-loop testing may be undesirable or impractical. For example, multirotor UAS are inherently unstable and always fly with an active automatic flight control system. Closed-loop operation has the potential to address these challenges as it increases stability, repeatability, and flexibility of flight tests and can be integrated into a fully automated procedure. Additionally, closed-loop operation can reduce the total flight test time, as bare-airframe, closed-loop, and broken-loop dynamics can all be identified from the same set of flight data. These advantages can lead to more accurate system identification results and reduce the time and efforts spent in flight testing, especially for small UAS.

Recently, several researchers have studied frequency response identification from closed-loop data. The lateral-directional dynamics of a small business jet were identified from closed-loop data in [3]. The control system created highly correlated aileron and rudder inputs, which was resolved using a joint input-output (JIO) frequency response estimator. In [4], the input correlation problem was addressed for orthogonal multisine inputs. In this case, feedback signals cause the separate control inputs to excite all harmonics, which are no longer orthogonal. This issue was

*M.S. Student, Department of Aerospace Engineering, University of Kansas, justinjmatt@gmail.com.
†Associate Professor, Department of Aerospace Engineering, University of Kansas, chaohaiyang@ku.edu.

resolved through interpolation of frequency responses to compensate for the effects of the correlated controls through feedback. The capability to identify bare-airframe, closed-loop, and broken-loop dynamics from closed-loop data was demonstrated in [5] by injecting programmed multisine signals at several points in the closed-loop system.

Other researchers have studied closed-loop system identification for small UAS. In [6], the JIO method was studied for multirotor UAS applications and best practices were recommended to mitigate the problem of input correlation. In [7], system identification results from open-loop and closed-loop data were compared experimentally for a fixed-wing UAS, using frequency-response based methods [8]. Following this same approach, frequency responses of a multirotor UAS were identified in [9].

These works effectively address the input correlation problem and show experimentally that UAS frequency responses can be identified from closed-loop data. In this paper, methods are presented to identify bare-airframe, closed-loop, and broken-loop frequency responses from the same set of closed-loop flight data, which can greatly reduce flight test time. This approach is particularly useful for small UAS that face challenges repeating system identification maneuvers at the same flight condition, which is critical for accurate frequency response identification. The methods discussed are demonstrated through flight simulation of a small, flying-wing UAS in strong turbulence. In this environment, open-loop system identification maneuvers may result in poor data quality or a loss of control, demonstrating the usefulness of this approach.

This paper is organized as follows. Section II provides a background on frequency response measurement and introduces the JIO frequency response estimator for systems operating in closed-loop. In Section III, the benefits of closed-loop flight testing for small UAS system identification are discussed, and methods are presented to identify bare-airframe, closed-loop, and broken-loop frequency responses from the same flight data set. A simulation example of a small, fixed-wing UAS flying in strong turbulence is presented in Section IV, and conclusions and future directions for this work are discussed in Section V.

II. Background

The theories of frequency response measurement, estimation, and system identification have been widely studied and applied in many different fields. In this section, a brief background on the frequency response estimators studied in this paper is provided. A generic system is considered and shown in Fig. 1, where u is the input signal, r is the reference signal, and y is the output signal. The best practice for frequency response measurement will be different depending on whether the system is operating in open- or closed-loop.

A. Open-loop Experiments

Under open-loop conditions, the frequency response can be measured directly from the input and output signals. If periodic excitation signals are used, such as multisine inputs, the frequency response can be measured directly from the discrete Fourier transform (DFT) at the excited frequencies, ω_k.

$$\hat{G}_{uy}(j\omega_k) = \frac{Y(j\omega_k)}{U(j\omega_k)} \tag{1}$$

If the signals are averaged over multiple periods, Eq. (1) is the maximum likelihood solution assuming Gaussian disturbances and is the best linear approximation of the underlying nonlinear system given periodic inputs [10]. This approach has often been applied to aircraft frequency response identification problems by programming mutually orthogonal multisine inputs into an automatic flight control system, which enables efficient flight testing and real-time frequency response estimation [11–13].

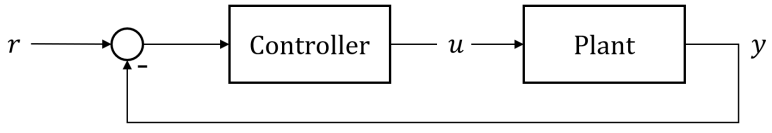

Fig. 1 General closed-loop system for reference signal tracking.

If non-periodic excitation signals are used, the frequency response can be measured using spectral estimation methods.

$$\hat{G}_{uy}(j\omega) = \frac{\hat{S}_{yu}(j\omega)}{\hat{S}_{uu}(j\omega)} \tag{2}$$

where $\hat{S}_{yu}(j\omega)$ and $\hat{S}_{uu}(j\omega)$ are estimates of the input-output cross-spectrum and input auto-spectrum. This estimate, sometimes called the H_1 solution, is unbiased so long as there is no input noise and is the best linear approximation of the underlying nonlinear system for arbitrary inputs [10, 14]. The H_1 solution has been commonly utilized for aircraft and rotorcraft frequency response identification using piloted frequency sweeps, following the methods developed in [8] for generating smooth spectral estimates using composite windowing techniques.

B. Closed-loop Experiments

Under closed-loop conditions, the previous estimators may break down because of noise feedback. In the presence of any nonlinearities or output noise, feedback causes $u(t)$ to become non-periodic, violating Eq. (1), while Eq. (2) becomes biased due to correlation between the input and output disturbances. The bias can be avoided using a joint input-output (JIO)* estimate of the frequency response [10, 16].

$$\hat{G}_{uy}(j\omega) = \frac{\hat{G}_{ry}(j\omega)}{\hat{G}_{ru}(j\omega)} \tag{3}$$

where $\hat{G}_{ry}$ is the frequency response from the reference to output and $\hat{G}_{ru}$ is the frequency response from the reference to input. These frequency responses can be computed using Eq. (1) or (2), depending on the periodicity of the reference signal. The JIO estimate is the best linear approximation of a nonlinear system operating in closed-loop [10, 17]. This estimate has been successfully employed in several recent works [3, 6, 18, 19] to identify bare-airframe frequency responses for multi-input flight control systems with highly correlated controls.

C. Coherence

The coherence function is often used to assess the quality of a frequency response, as it measures the linear correlation between the measured input and output as a function of frequency. Coherence is defined as

$$\gamma^2_{uy}(j\omega) = \frac{|\hat{S}_{uy}(j\omega)|^2}{|\hat{S}_{uu}(j\omega)||\hat{S}_{yy}(j\omega)|} \tag{4}$$

For periodic signals, the coherence can be computed if the signal is measured over successive periods ($M > 1$) [10].

$$\gamma^2_{uy} = \frac{\left|\frac{1}{M}\sum_{i=1}^{M} Y_i(j\omega_k)\overline{U}_i(j\omega_k)\right|^2}{\left(\frac{1}{M}\sum_{i=1}^{M}|U_i(j\omega_k)|^2\right)\left(\frac{1}{M}\sum_{i=1}^{M}|Y_i(j\omega_k)|^2\right)} \tag{5}$$

If no averaging is used, the coherence is exactly 1 at all frequencies, and the coefficient of determination, R^2, is an analogous metric that can be used [20].

A method to estimate the coherence of a frequency response that is computed as a function of two other frequency responses, as in the JIO method, was developed in [3] and is adopted here. This method computes the coherence as the weighted minimum of the coherence of the two frequency responses.

$$\gamma^2_{uy}(j\omega) = W(x)\min(\gamma^2_{G_{ry}}, \gamma^2_{G_{ru}}) \tag{6}$$

where

$$W(x) = [1.582(1 - e^{-x})]^2 \tag{7}$$

*It should be noted that in some literature this estimate is classified as a JIO method [15], while in others it is classified as an indirect method [10]. We elect to refer to it as a JIO method to remain consistent with other aerospace literature [3].

$$x = \begin{cases} (\gamma^2_{G_{ry}} \gamma^2_{G_{ru}})^{1/2} & \text{if } \max(\gamma^2_{G_{ry}}, \gamma^2_{G_{ru}}) < 0.9 \\ z + (1 - z)(\gamma^2_{G_{ry}} \gamma^2_{G_{ru}})^{1/2} & \text{otherwise} \end{cases} \tag{8}$$

$$z = 10[\max(\gamma^2_{G_{ry}}, \gamma^2_{G_{ru}}) - 0.9] \tag{9}$$

In the weighting function in Eq. (7), x is the geometric mean of the two coherence functions if both values are below 0.9. Otherwise, x is interpolated between the geometric mean and 1, ensuring that the coherence collapses to the minimum if a single coherence is very high.

III. Application to Small UAS

A. Benefits of Closed-loop Flight Testing

Active feedback control has disadvantages for system identification that have historically led to most system identification flight tests being performed open-loop. The main drawbacks are the suppression of the excitation signal and the correlation of the input signal with noise and disturbances. However, closed-loop operation also provides some benefits when compared to open-loop flight testing. The primary benefits of closed-loop flight testing are

- Increased aircraft stability during system identification flight maneuvers which subsequently increases the flexibility of flight test design (less constraints on wind and gust levels);
- Capability to perform fully- or partially-automated system identification flight tests;
- Identification of bare-airframe, closed-loop, and broken-loop system dynamics from the same data set, reducing total flight test time.

These benefits are especially of interest for small UAS due to their unique challenges during system identification flight tests [21]. Increased stability during flight test allows for the design of larger flight maneuvers, resulting in higher signal-to-noise ratios (SNR) which are critical for accurate identification results. The capability to perform system identification flight tests with some level of automatic control is crucial for UAS that have built-in active feedback control functions, such as multirotor UAS. Furthermore, increased automation can make it easier to collect high-quality system identification data sets with longer data length, which increases frequency resolution and can improve identification results, especially at low frequencies. In fact, UAS system identification flight tests are typically constrained by the pilot's visual line-of-sight or the range of radio links.

Finally, closed-loop flight testing allows for the identification of bare-airframe, closed-loop, and broken-loop system dynamics from the same data set. This is particularly useful for small UAS, as flight tests are typically repeated at the same trim condition to identify the different loop dynamics. Repeating flight maneuvers in this way is difficult for small UAS, as these aircraft often lack accurate real-time airspeed measurements. Additionally, changes in wind direction or speed can create significant changes in the low UAS cruise speed. As such, identifying the system dynamics from the same closed-loop flight data set can lead to improved identification accuracy and a reduction in flight test time.

B. UAS Frequency Response Identification

In this section the procedure for measuring small UAS frequency responses from closed-loop flight data is outlined. Methods for measuring frequency responses describing the bare-airframe, closed-loop, and broken-loop dynamics from a single flight data set are discussed. The measured closed-loop and broken-loop frequency responses can be compared to theoretical values computed from an identified, parametric bare-airframe model, providing experimental validation of the closed-loop system.

A roll tracking controller, pictured in Fig. 2, is used as an example. The control objective is to drive the roll angle and roll rate to the commanded values, ϕ_c and p_c. The control input is the aileron deflection, δ_a. The controller includes a feedback loop that provides stabilization and a feed-forward loop that provides baseline open-loop tracking. This type of control structure is simple but effective and is popular with open-source autopilots (e.g., ArduPlane, PX4) designed for small, low-cost UAS as the gains can readily be tuned in flight using heuristic methods [2].

A critical step for closed-loop system identification is the design of the reference signal. The reference signal should be designed to sufficiently excite both the input signal, δ_a, and the system output signals. In this example, we have two external signals, ϕ_c and p_c, that could be used as the reference signal. Often, p_c is computed as a function of ϕ_c. For this reason, design of the roll angle command signal, ϕ_c, is the primary design consideration for flight testing.

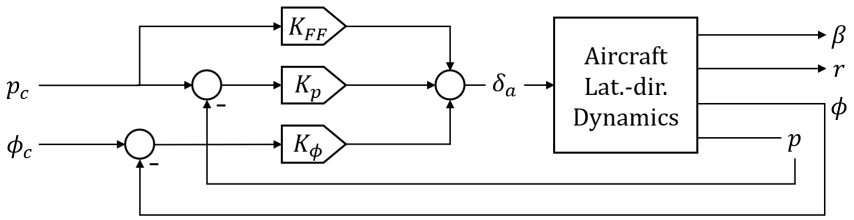

Fig. 2 Roll angle tracking controller.

1. Bare-airframe Dynamics

The open-loop frequency response can be computed from Eq. (3) for each output signal. If the controller has multiple reference signals, as in Fig. 2, there are several options for the reference signal. In some cases, the following approximation might be made:

$$p_c \approx \dot{\phi}_c \tag{10}$$

In this case, either ϕ_c or p_c could be selected as the reference. However, if the two commands are nonlinearly related, the nonlinearities will introduce errors in the measured frequency responses. Then, the combination of feed-forward elements is a more suitable choice for reference signal.

$$r(t) = (K_p + K_{FF})p_c(t) + K_\phi \phi_c(t) \tag{11}$$

2. Closed-loop System Dynamics

The closed-loop system dynamics can be measured from flight data and compared to theoretical transfer functions computed from identified, parametric bare-airframe models. The lateral-directional closed-loop dynamics are primarily characterized by the roll angle response to roll angle command. The equation describing this response is dependent on the relationship between the two command signals, ϕ_c and p_c. First, assuming $p \approx \dot{\phi}$ and $p_c \approx \dot{\phi}_c$, the closed-loop transfer function (CLTF) for roll command tracking can be fully described by a single-input, single-output (SISO) system.

$$\left[\frac{\phi}{\phi_c}(s)\right]_{\text{SISO}} = \frac{G(s)(K_\phi + sK_p + sK_{FF})}{s + G(s)(K_\phi + sK_p)} \tag{12}$$

where $G(s)$ is used to denote the aileron-to-roll rate transfer function, $p/\delta_a(s)$.

If p_c is not or cannot be approximated as a linear function of ϕ_c (e.g., because of command saturation), the roll angle response can be written as a multi-input, single-output (MISO) system.

$$\phi(s) = \left[\frac{\phi}{\phi_c}(s)\right]\phi_c(s) + \left[\frac{\phi}{p_c}(s)\right]p_c(s) \tag{13}$$

The two inputs to Eq. (13) are likely high correlated, making it difficult to measure the individual contributions of each. One method to measure the MISO frequency response $\phi/\phi_c(j\omega)$ from flight data is to subtract out the estimated influence of the additional input, denoted ϕ_{p_c}.

$$\frac{\phi}{\phi_c}(j\omega) = \frac{[\phi - \phi_{p_c}](j\omega)}{\phi_c(j\omega)} \tag{14}$$

This can be estimated by passing p_c through the roll rate command-to-roll angle transfer function, $\hat{G}_{p_c\phi}(s)$, which is computed from a parametric estimate of the aileron-to-roll rate transfer function, $\hat{G}(s)$.

$$\phi_{p_c}(s) = \hat{G}_{p_c\phi}(s)p_c(s) = \left[\frac{\hat{G}(s)(K_{FF} + K_p)}{s + \hat{G}(s)(K_\phi + sK_p)}\right]p_c(s) \tag{15}$$

The arithmetic in the numerator of Eq. (14) can be performed in the time domain by subtracting the signals or in the frequency domain by decomposing the fraction into the difference between two separate frequency responses. The equivalent transfer function used for comparison is

$$\left[\frac{\phi}{\phi_c}(s)\right]_{\text{MISO}} = \frac{G(s)K_\phi}{s + G(s)(K_\phi + sK_p)} \tag{16}$$

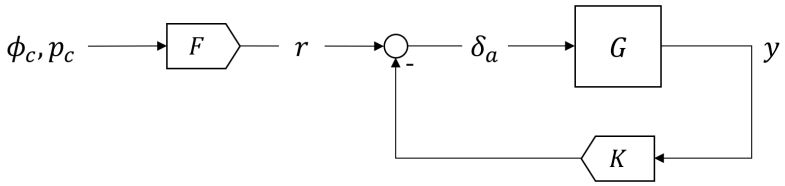

Fig. 3 Simplified block diagram of the roll tracking controller showing the loop gain, GK.

3. Broken-loop Dynamics

Broken loops are obtained by breaking a SISO loop at a particular point while leaving the other loops closed. These loops are of interest to flight control engineers as they provide a means for analysis of stability margins and disturbance rejection capability [8, 22, 23]. The broken loops can be more easily visualized by rearranging the block diagram to the simplified structure in Fig. 3.

Stability margins are measured from the loop gain, $GK(s)$, where G is the forward loop and K is the feedback loop. To remain consistent with Ref. [24], a single loop is defined for each "force or moment producer." Thus, we treat the loop as a SISO system where $G(s) = p/\delta_a(s)$, and the theoretical loop gain is computed as

$$GK(s) = G(s)(K_\phi/s + K_p) \tag{17}$$

The loop gain is commonly measured from flight data by injecting an excitation signal at the servo command. When closed-loop testing is performed for identifying the bare-airframe dynamics, the reference signal, r, breaks the loop. Thus, the same data set can be used to measure the loop gain. An indirect approach is preferred as the measured response will be unbiased for output noise [8, 25]. From Fig. 3, the error response is

$$\frac{\delta_a}{r}(s) = [1 + GK(s)]^{-1} \tag{18}$$

This response can be measured from flight data using Eq. (1) or (2). Then, the broken-loop response can be computed algebraically in the frequency domain.

$$GK(j\omega) = \left[\frac{\delta_a}{r}(j\omega)\right]^{-1} - 1 \tag{19}$$

Broken loops are also used to measure output sensitivity functions, which are used to characterize the aircraft's ability to attenuate disturbances. This is typically measured by injecting a disturbance signal into the feedback path of the hold variable, i.e., roll angle, while the controller is in a hold mode. The sensitivity function is defined by

$$S_o(s) = [I + GK(s)]^{-1} \tag{20}$$

which is the multi-input multi-output (MIMO) equivalent to Eq. (18). The sensitivity function is typically computed for each feedback variable individually, which is consistent with MIMO analysis [23]. Thus, we are interested in solely the roll angle output and feedback, and our theoretical SISO transfer function used for comparison is

$$S_{o_\phi}(s) = \left[1 + \frac{G(s)}{s}K_\phi\right]^{-1} = 1 - \frac{G(s)K_\phi}{s + G(s)(K_\phi + sK_p)} \tag{21}$$

Thus, the sensitivity function can be reconstructed from the measured CLTF.

$$S_{o_\phi}(j\omega) = 1 - \frac{\phi}{\phi_c}(j\omega) \tag{22}$$

where $\phi/\phi_c(j\omega)$ is computed using Eq. (16) to be consistent with our MIMO-definition of the sensitivity function.

Two metrics, the disturbance rejection bandwidth (DRB) and disturbance rejection peak (DRP), are computed from the hold variable sensitivity function. DRB is defined as the frequency at which the magnitude of S_{o_ϕ} crosses -3 dB from below, and DRP is defined as the peak gain of the sensitivity function. These metrics characterize the aircraft's response to disturbances.

IV. Simulation Example

A simulation example is provided to demonstrate the methods outlined in the previous sections. First, the simulation environment is described, which was designed to represent flight testing conditions that make open-loop testing difficult for small UAS system identification. Then, simulation results are presented.

A. Simulation Environment

A flight simulation environment was developed for a small, flying-wing UAS. The simulation environment includes several submodules to attempt to mimic real flight conditions. The overall system architecture is shown in Fig. 4.

1. UAS Dynamic Model

The Zephyr3-R UAS was used for simulation. The Zephyr3-R is a small, flying-wing UAS with elevon controls, pictured in Fig. 5. The Zephyr3-R has a mass of 2.2 kg and wingspan of 122 cm. The lateral-directional dynamics were identified from flight test data at a trim airspeed of 15 m/s [21]. The dynamics are given in linear state space form:

$$\begin{bmatrix} \dot{v} \\ \dot{p} \\ \dot{r} \\ \dot{\phi} \end{bmatrix} = \begin{bmatrix} Y_v & Y_p + W_0 & Y_r - U_0 & g\cos\Theta_0 \\ L_v & L_p & L_r & 0 \\ N_v & N_p & N_r & 0 \\ 0 & 1 & \tan(\Theta_0) & 0 \end{bmatrix} \begin{bmatrix} v \\ p \\ r \\ \phi \end{bmatrix} + \begin{bmatrix} 0 \\ L_{\delta_a} \\ 0 \\ 0 \end{bmatrix} \delta_a(t-\tau) \tag{23}$$

State space model parameters are given in Table. 1

2. Command and Control Modules

Automated frequency sweeps were generated as the roll command signal to excite the lateral-directional dynamics. The roll rate command was computed by Eq. (10) and saturated at ±75 deg/s. The signal increased in frequency exponentially from 1.0 to 35 rad/s over a 25 second period and was generated using the equations listed in [8]. The command signal had an amplitude of ±15 degrees. These parameters were selected based on previous flight test results [21]. Two simulated maneuvers were used for system identification.

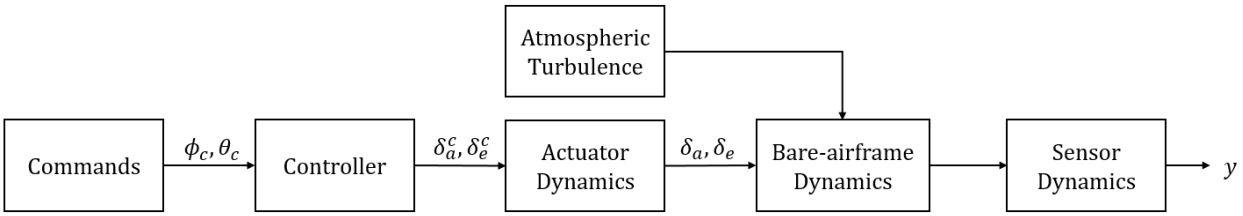

Fig. 4 Simulation environment structure.

Fig. 5 KHawk Zephyr3-R UAS.

Table 1 Zephyr3-R UAS state space model parameters.

Parameter	Value	Units	Parameter	Value	Units	Parameter	Value	Units
U_0	17	m/s	Y_r	0.6274	m/s	N_p	-0.7187	s^{-1}
W_0	0.9	m/s	L_v	-0.8447	$(m\ s)^{-1}$	N_r	-1.509	s^{-1}
Θ_0	3	deg	L_p	-8.569	s^{-1}	L_{δ_a}	170.0	s^{-2}
Y_v	-0.6868	s^{-1}	L_r	3.133	s^{-1}	τ	0.0548	s
Y_p	0.1649	m/s	N_v	0.8419	$(m\ s)^{-1}$			

The roll tracking control system follows the structure shown in Fig. 2. Gains were tuned heuristically based on noisy simulation data in attempt to mimic real flight test scenarios. The feed-forward gain was tuned first from open-loop step commands, then feedback gains were tuned to track a roll angle step command. Gains were selected to provide a fast response with low steady state error and small overshoot (<10%). The selected gains are

$$K_P = 0.2 \qquad K_{FF} = 0.033 \qquad K_D = 0.01 \tag{24}$$

3. Actuator Dynamics

A first-order transfer function model was used to simulate the actuator dynamics. This model was identified from ground test measurements of the Zephyr3-R elevon deflection [26].

$$\frac{\delta_{a,e}}{\delta^c_{a,e}} = \frac{1}{0.032s + 1} \tag{25}$$

4. Atmospheric Turbulence

The low-altitude Dryden turbulence model was used to simulate atmospheric turbulence and was implemented using the MATLAB & Simulink Aerospace Blockset[†]. Turbulence intensity is computed from the flight altitude and wind speed at 6 meters above ground level (AGL). The UAS was simulated to fly at an altitude of 100 meters, and the wind speed at 6 meters AGL was selected as 30 knots, which is typically defined as representing moderate turbulence for manned aircraft [22]. For a small UAS, this more accurately represents strong turbulence that is not suitable for open-loop system identification flight tests.

5. Sensor Dynamics

Sensor noise was simulated for accelerometer, gyroscope, and attitude angle measurements. Gaussian white noise was generated for the accelerometer and gyroscopes, with variance selected from ground test experiments. The accelerometer and gyroscope noise standard deviation are $\sigma_{\text{acc}} = 0.01$ m/s^2 and $\sigma_{\text{gyro}} = 0.04$ deg/s.

As attitude angles are typically estimated using an extended Kalman filter, low-frequency, colored noise was simulated as measurement noise, based on ground experiments. The colored noise was generated by filtering Gaussian white noise ($\sigma_{\text{att}} = 0.06$ deg) with a first-order low-pass filter with cutoff frequency of 0.1 rad/s.

B. Simulation Results

Two roll frequency sweep maneuvers were simulated and used to compute frequency responses. Time histories of the aircraft response and controller commands are shown in Fig. 6. Significant disturbances due to turbulence are visible throughout the data, particularly in the five seconds prior to the maneuver.

The identified bare-airframe, closed-loop, and broken-loop frequency responses are computed from spectral function estimates generated by CIFER®. Then, a parametric aileron-to-roll rate transfer function model is identified and used to compute parametric models of the closed-loop and broken-loop dynamics. Specific parameters and metrics are compared between the identified and true responses. Additionally, a quadratic cost function, J, is used to compare results. The cost function quantifies the weighted sum of squared magnitude and phase errors between the identified and

[†]Aerospace Blockset - MATLAB & Simulink. https://www.mathworks.com/products/aerospace-blockset.html. Accessed June 2022.

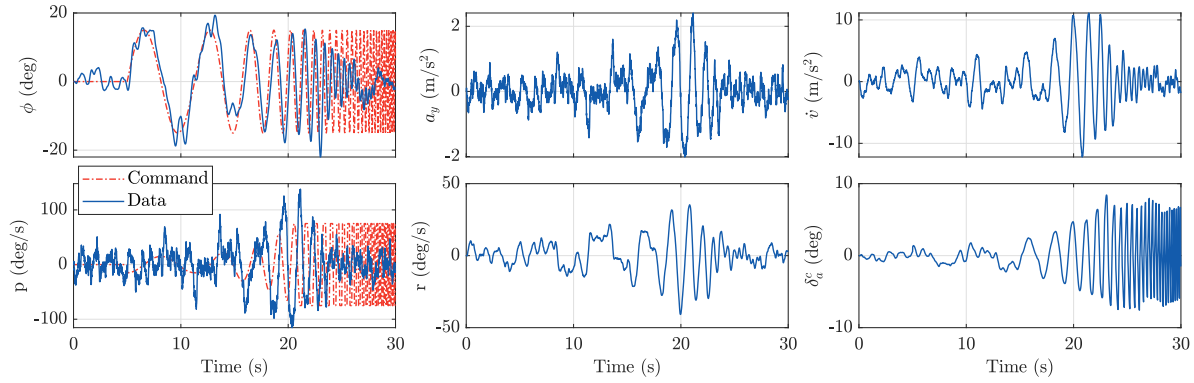

Fig. 6 Time-history of simulated roll command frequency sweep.

Table 2 Identified p/δ_a transfer function parameters.

Parameter	Units	Model	Truth	Percent Error (%)
L_{δ_a}	s^{-2}	161	170	5.3
ζ_ϕ	-	0.28	0.31	9.7
ω_ϕ	rad/s	3.5	3.6	3
L_p	s^{-1}	7.9	-8.4	6
ζ_{dr}	-	0.30	0.31	3.2
ω_{dr}	rad/s	3.9	4.0	3
τ	s	0.052	0.055	5.5

true responses [8]. Generally, cost function values below 50 indicate excellent agreement between responses. Listed cost function values were computed over the frequency range of ω = 1–20 rad/s unless otherwise stated.

Bare-airframe frequency responses for roll rate, yaw rate, lateral acceleration, and lateral velocity derivative were generated using Eq. (3). The computed frequency responses are shown in Fig. 7 and compared with the true transfer functions computed from the state space model. Each of the four measured frequency responses matches well with the true response. High coherence over a wide frequency band further indicates the quality of the simulation data. This band covers the primary lateral-directional dynamics of interest. As such, parametric models fit to the measured frequency responses are expected to be highly accurate.

A transfer function was identified to fit the measured aileron-to-roll rate frequency response. A third-order transfer function with time delay was identified, corresponding with the three degree-of-freedom Dutch-roll approximation that neglects the spiral dynamics [27]. This structure is useful as most aircraft have an unstable spiral mode, which would give a divergent result when reconstructing the signal in Eq. (15). The transfer function takes the form

$$\frac{p}{\delta_a} = \frac{L_{\delta_a}(s^2 + 2\zeta_\phi\omega_\phi s + \omega_\phi^2)}{(s - L_p)(s^2 + 2\zeta_{dr}\omega_{dr} s + \omega_{dr}^2)} e^{-\tau s} \tag{26}$$

The transfer function was fit to the frequency response over the frequency range of ω = 1–32 rad/s using the NAVFIT module in CIFER®, which estimates transfer function parameters by minimizing the cost function, J. The identified transfer function is pictured in Fig. 8, and the parameters are listed in Table 2. The cost function is computed over the fitting frequency range and indicates an excellent fit.

The identified roll rate model was used to compute the theoretical closed-loop dynamics and compared with measured simulation data. The closed-loop transfer function was identified using Eq. (14) because of the nonlinearity (saturation) present in the computation of p_c. The measured, modeled, and true frequency responses are shown in Fig. 9. The responses show high coherence and a good fit with the truth over a wide frequency range.

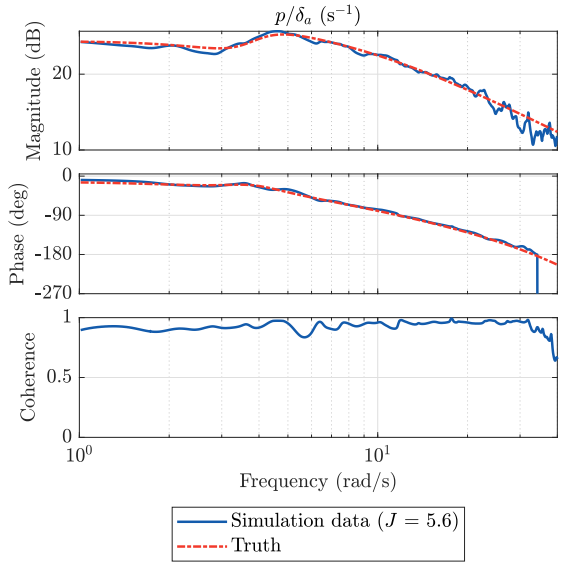

(a) Aileron to roll rate, p/δ_a, frequency response

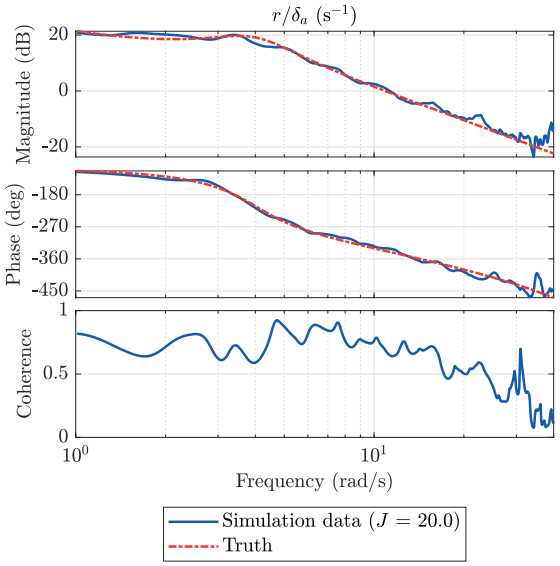

(b) Aileron to yaw rate, r/δ_a, frequency response

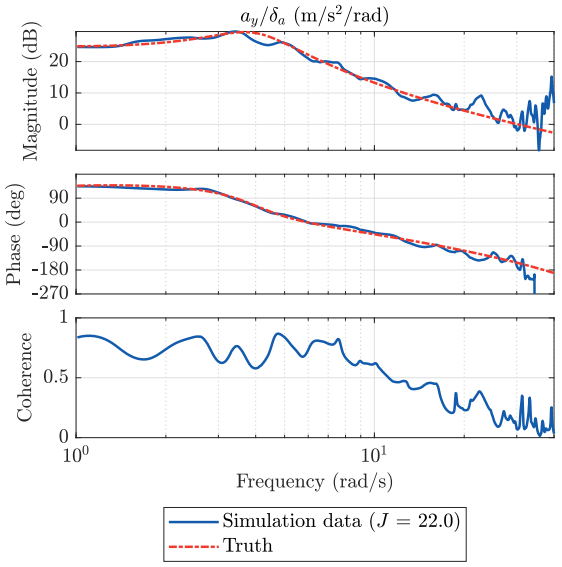

(c) Aileron to lateral acceleration, a_y/δ_a, frequency response

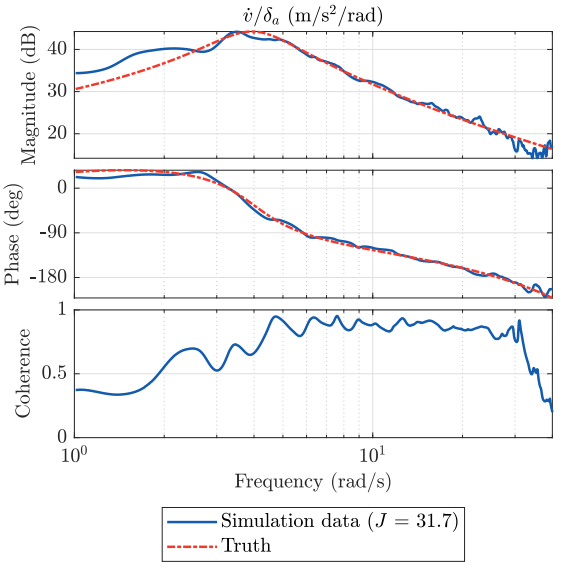

(d) Aileron to y-axis body velocity derivative, $\dot{v}/\delta_a$, frequency response

Fig. 7 Measured bare-airframe frequency responses compared to truth model.

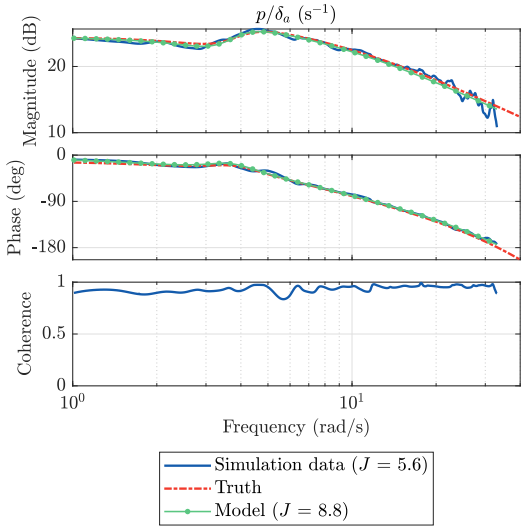

Fig. 8 Aileron-to-roll rate transfer function, p/δ_a, comparison.

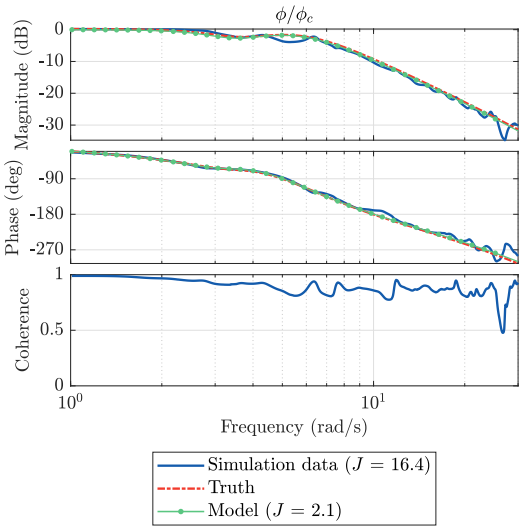

Fig. 9 Closed-loop transfer function, ϕ/ϕ_c, comparison.

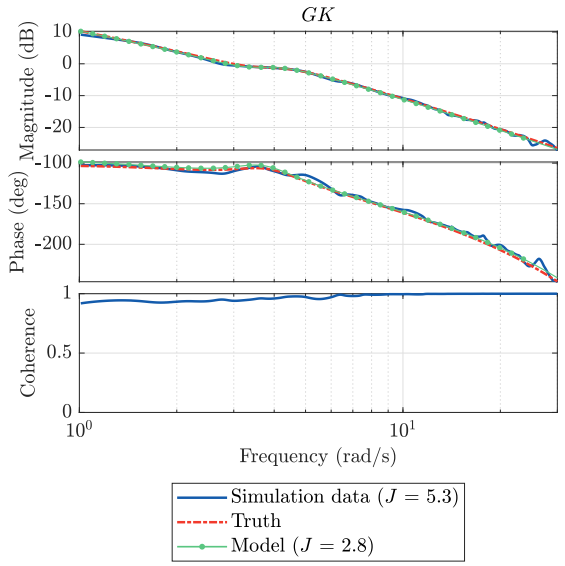

Fig. 10 Loop gain transfer function, GK, comparison.

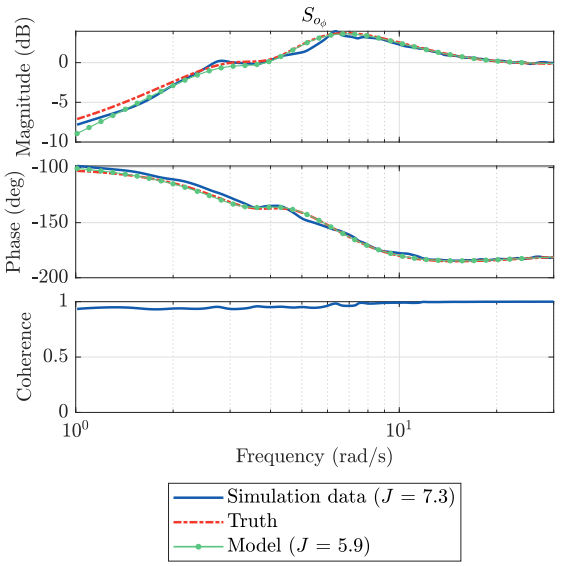

Fig. 11 Roll angle sensitivity function, S_{o_ϕ}, comparison.

The loop gain and output sensitivity functions were computed from the simulation data using Eqs. (19) and (22). The measured frequency responses are compared to the modeled and true responses in Fig. 10 and 11. The measured, modeled, and true responses all match very closely across a wide frequency range. The broken loop crossover frequencies, stability margins, and the disturbance rejection metrics of the three responses are compared in Table 3. For both the simulation data and model, each metric was identified within 9% of the true value.

This simulation example demonstrated the usefulness of the described methods for small UAS frequency response identification. Simulated flight data was generated in the presence of strong turbulence, which makes open-loop flight testing of small UAS difficult. Bare-airframe dynamics, closed-loop and broken-loop frequency responses were identified accurately from closed-loop flight data. A parametric model was fit to the aileron-to-roll rate frequency response and used to compute parametric models of the closed- and broken-loop frequency responses. The measured, modeled, and true frequency responses showed excellent agreement over a wide frequency range, as indicated by the low cost function values and low error between true and identified parameters.

Table 3 Identified closed-loop system characteristics.

Parameter	Units	Simulation Data	Model	Truth
Loop gain crossover frequency	rad/s	2.73	2.86	2.98
Loop phase crossover frequency	rad/s	14.3	14.0	13.7
Loop gain margin	dB	16.3	16.1	15.2
Loop phase margin	deg	67.0	76.0	72.5
Disturbance rejection bandwidth	rad/s	1.98	1.94	1.82
Disturbance rejection peak	dB	3.95	3.63	3.71
Disturbance rejection peak frequency	rad/s	6.36	6.85	6.83

V. Conclusion

This paper presented a method to identify bare-airframe, closed-loop, and broken-loop frequency responses from the same set of closed-loop flight data. This approach is particularly useful for small UAS, which have unique system identification challenges due to their small size, low-speed, and often low-cost nature. The closed-loop methods described can improve flight test stability, flexibility, and repeatability, allow for fully- or partially- autonomous flight tests, and reduce total flight test time. Additionally, identifying the bare-airframe, closed-loop, and broken-loop dynamics from the same data set is particularly useful for small UAS, as, typically, flight tests are repeated at the same trim condition for each loop. For small UAS, this can be difficult as small changes in wind speed or direction can significantly affect the current flight condition.

The methods discussed in this paper were demonstrated through simulation of the Zephyr3-R UAS flying under strong turbulence conditions. This represents a situation where open-loop flight testing would be very difficult. Accurate models were identified from two sets of closed-loop frequency sweep simulation data. A total of 50 seconds of simulation data was used to fully identify the open-, closed, and broken-loop lateral-directional dynamics of the UAS, showing the usefulness of the described methods. In the future, the methods discussed in this paper will be applied to small UAS flight data.

Acknowledgements

This work is supported in part by the Army Research Lab Grant W911NF-22-2-027, the USDA-NIFA Grant 2019-67021-28992, and the University of Kansas School of Engineering Research and Innovation Seed (RISe) Funding.

References

[1] Flanagan, H. P., Hagerott, S. G., and Chao, H., "Model Based Roll Controller Tuning and Analysis for Small UAS in Turbulent Environments," *2018 International Conference on Unmanned Aircraft Systems (ICUAS)*, 2018, pp. 1398–1407. https://doi.org/10.1109/ICUAS.2018.8453442.

[2] Matt, J. J., Flanagan, H., and Chao, H., "Evaluation and Analysis of ArduPilot Automatic Tuning Algorithm for the Roll Tracking Controller of a Small UAS," *AIAA Scitech 2021 Forum*, 2021. https://doi.org/10.2514/6.2021-0016.

[3] Berger, T., Tischler, M. B., Knapp, M. E., and Lopez, M. J. S., "Identification of Multi-Input Systems in the Presence of Highly Correlated Inputs," *Journal of Guidance, Control, and Dynamics*, Vol. 41, No. 10, 2018, pp. 2247–2257. https://doi.org/10.2514/1.G003530.

[4] Grauer, J. A., and Boucher, M. J., "Real-Time Estimation of Bare-Airframe Frequency Responses from Closed-Loop Data and Multisine Inputs," *Journal of Guidance, Control, and Dynamics*, Vol. 43, No. 2, 2020, pp. 288–298. https://doi.org/10.2514/1.G004574.

[5] Grauer, J. A., "Frequency Response Estimation for Multiple Aircraft Control Loops Using Orthogonal Phase-Optimized Multisine Inputs," *Processes*, Vol. 10, No. 4, 2022. https://doi.org/10.3390/pr10040619.

[6] Berger, T., Lopez, M. J. S., and Tischler, M. B., "Guidelines for System Identification of Multirotor Vehicles with Highly Correlated Inputs," *VFS 76th Annual Forum*, 2020. https://doi.org/10.4050/F-0076-2020-16294.

[7] Babcock, J. T., Osteroos, R. K., and Tischler, M. B., "Open and Closed Loop System Identification of the Stryker 200 UAV," *AIAA SCITECH 2022 Forum*, 2022. https://doi.org/10.2514/6.2022-2405.

[8] Tischler, M., and Remple, R., *Aircraft And Rotorcraft System Identification: Engineering Methods With Flight-test Examples*, 2nd ed., AIAA, Reston, VA, 2016.

[9] Gong, A., Sanders, F. C., Hess, R. A., and Tischler, M. B., "System Identification and Full Flight-Envelope Model Stitching of a Package-Delivery Octocopter," *AIAA Scitech 2019 Forum*, 2019. https://doi.org/10.2514/6.2019-1076.

[10] Pintelon, R., and Schoukens, J., *System Identification: A Frequency Domain Approach*, 2nd ed., Wiley, Hoboken, NJ, 2012.

[11] Morelli, E. A., and Klein, V., *Aircraft System Identification: Theory and Practice*, 2nd ed., Sunflyte, Williamsburg, VA, 2016.

[12] Morelli, E. A., "Multiple input design for real-time parameter estimation in the frequency domain," *IFAC Proceedings Volumes*, Vol. 36, No. 16, 2003, pp. 639–644. https://doi.org/https://doi.org/10.1016/S1474-6670(17)34833-4.

[13] Grauer, J., and Morelli, E., "Method for Real-Time Frequency Response and Uncertainty Estimation," *Journal of Guidance, Control, and Dynamics*, Vol. 37, No. 1, 2014, pp. 336–344. https://doi.org/10.2514/1.60795.

[14] Bendat, J. S., and Piersol, A. G., *Engineering Applications of Correlations and Spectral Analysis*, Wiley, New York, NY, 1980.

[15] Ljung, L., *System Identification: Theory for the User*, 2nd ed., Prentice Hall, Upper Saddle River, NJ, 1999.

[16] Akaike, H., "Some Problems in the Application of the Cross-Spectral Method," *Spectral Analysis of Time Series*, 1967, pp. 81–107.

[17] Pintelon, R., and Schoukens, J., "FRF Measurement of Nonlinear Systems Operating in Closed Loop," *IEEE Transactions on Instrumentation and Measurement*, Vol. 62, No. 5, 2013, pp. 1334–1345. https://doi.org/10.1109/TIM.2012.2220033.

[18] Knapp, M. E., Berger, T., Tischler, M., and Cotting, M. C., *Development of a Full Envelope Flight Identified F-16 Simulation Model*, 2018. https://doi.org/10.2514/6.2018-0525.

[19] Berrigan, C., Lopez, M. J. S., Ruckel, P., and Prasad, J. V. R., "Bell V-280 System Identification and Model Vali- dation with Flight Test Data using the Joint Input-Output Method," *VFS 76th Annual Forum*, 2020. https://doi.org/10.4050/F-0076-2020-16393.

[20] Morelli, E. A., and Grauer, J. A., "Practical Aspects of Frequency-Domain Approaches for Aircraft System Identification," *Journal of Aircraft*, Vol. 57, No. 2, 2020, pp. 268–291. https://doi.org/10.2514/1.C035599.

[21] Matt, J. J., Hagerott, S. G., Svoboda, B. C., Chao, H., and Flanagan, H. P., "Frequency Domain System Identification of a Small Flying-Wing UAS," *AIAA SCITECH Forum*, 2022. https://doi.org/10.2514/6.2022-2407.

[22] anon., "Flying Qualities of Piloted Aircraft," Tech. Rep. MIL-HDBK-1797B, U.S. Department of Defense, 2012.

[23] Berger, T., Ivler, C., Berrios, M., Tischler, M., and Miller, D., "Disturbance Rejection Handling Qualities Criteria for Rotorcraft," *AHS 72nd Annual Forum*, 2016.

[24] anon., "Flight Control Systems - Design, Installation, and Test of Piloted Aircraft, General Specification for," Tech. Rep. MIL-F-9490D, U.S. Department of Defense, 1964.

[25] McCoy, A. H., "Flight Testing and Real-Time System Identification Analysis of a UH-60A Black Hawk Helicopter with an Instrumented External Sling Load," *M.S. Thesis, Naval Post Graduate School, Dept. of Aeronautical Engineering*, 1997.

[26] Matt, J. J., Chao, H., Shawon, M. H., and Hagerott, S. G., "Longitudinal System Identification for a Small Flying-wing UAS," *AIAA Scitech 2023 Forum (to appear)*, 2023.

[27] McRuer, D., Ashkenas, I., and Graham, D., *Aircraft Dynamics and Automatic Control*, Princeton University Press, 1973.